Materials Advances

ROYAL SOCIETY OF CHEMISTRY

PAPER

View Article Online
View Journal | View Issue

Check for updates

Cite this: *Mater. Adv.*, 2023, 4, 6277

Red fluorescent carbon nanoparticles derived from *Spinacia oleracea L.*: a versatile tool for bioimaging and biomedical applications†

Ketki Barve,‡[a] Udisha Singh,‡[b] Pankaj Yadav,‡[b] Krupa Kansara,[b] Payal Vaswani,[b] Ashutosh Kumar [c] and Dhiraj Bhatia *[b]

Received 30th May 2023,
Accepted 20th October 2023

DOI: 10.1039/d3ma00273j

rsc.li/materials-advances

Carbon-based fluorescent nanoparticles are an emerging class of nanoparticles for targeted bioimaging and biomedical applications. We present a facile microwave-assisted approach for synthesizing carbon nanoparticles with bright red fluorescence using ethanolic extracts of *Spinacia oleracea* leaves, with a quantum yield of 94.67%. These nanoparticles, called CNPs, of size 98 ± 20 nm, demonstrated fluorescence emission in the near-infrared (NIR) region between 650 and 700 nm, independent of the excitation wavelength. Upon excitation at a wavelength of 410 nm, they exhibit an emission maximum peak at 672 nm. The significant uptake of CNPs by mammalian cells and zebrafish larvae highlights their potential as a bioimaging agent in diverse biomedical applications *in vivo*. Furthermore, these quantum dots enhance cellular proliferation and migration as observed by wound healing assay in mammalian cells, indicating their possible application in tissue engineering and regenerative medicine. These findings suggest that the biosynthesized carbon nanoparticles possess significant potential for biomedical applications, which can serve as a robust benchmark for researchers towards promoting sustainability.

Open Access Article. Published on 20 October 2023. Downloaded on 1/9/2025 7:18:45 PM.
This article is licensed under a Creative Commons Attribution 3.0 Unported Licence.

1. Introduction

Nanoparticles have garnered much interest in recent years due to their distinctive physical and chemical characteristics. Carbon nanoparticles, in particular, have been of great interest in various fields, including targeted therapeutics, biosensing,[1–3] theranostics, bioimaging, and photodynamic therapy (PDT), owing to their biocompatibility, low toxicity, and high stability. Top-down and bottom-up methods are two types of methods of synthesis of nanoparticles.[4] The bottom-up method enables a precise control of the size and shape of the nanoparticles. Various bottom-up methods are used for the synthesis of nanoparticles, for example, microwave,[5] hydrothermal,[6,7] and reflux.[8] The microwave method of synthesis offers great advantages over the other methods in terms of a high reaction rate and energy efficient and localized heating of precursors in a short interval of time (within minutes), thereby precisely controlling the shape and size of the nanoparticles.

Carbon-based nanoparticles possess distinct optical properties and surface modifications due to their unique size and structure. They can be used as contrast agents for imaging biological entities such as cells and tissues. Their small size and biocompatibility also make them suitable for the targeted delivery of drugs to specific cells or tissues. The optical characteristics of CNPs are dependent on the band gap energy. Upon absorption of light at a particular wavelength corresponding to the band gap energy, the valence band electrons of these nanoparticles undergo a quick transition to the conduction band and return to the valence band by releasing energy in the form of light or photons. Compared to chemical substances (such as citric acid, glucose, urea, and thiourea) used to make CNPs, the synthesis of CNPs using natural materials has many benefits since they are less expensive, non-toxic, and more abundant.[9] Consequently, there is a need to investigate easily accessible and cost-effective carbon sources using environmentally friendly green technologies to synthesize high-quality carbon-based nanoparticles with superior photoluminescence (PL) properties.[10–12]

In this regard, spinach extract comprises bio-reductants, including flavonoids, polyphenols, amino acids, and carbohydrates, that stabilize nanoparticle synthesis and mitigate agglomeration.[13] Its application in medicine involves injecting

[a] *Dr D. Y. Patil Biotechnology and Bioinformatics Institute, Dr. D. Y. Patil Vidyapeeth, Pune, Maharashtra, 411018, India*
[b] *Department of Biological Sciences and Engineering, Indian Institute of Technology Gandhinagar, Palaj, Gujarat 382355, India. E-mail: dhiraj.bhatia@iitgn.ac.in*
[c] *Biological and Life Sciences, School of Arts and Sciences, Ahmedabad University, Navrangpura, Ahmedabad, India*

† Electronic supplementary information (ESI) available. See DOI: https://doi.org/10.1039/d3ma00273j

‡ The authors contributed equally.

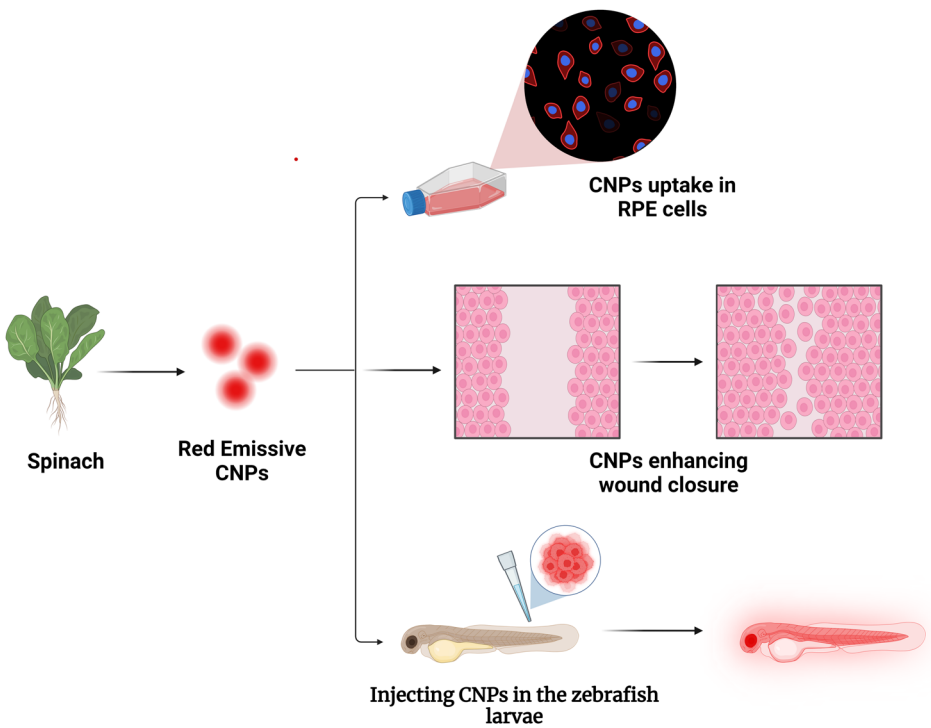
© 2023 The Author(s). Published by the Royal Society of Chemistry

Open Access Article. Published on 20 October 2023. Downloaded on 1/9/2025 7:18:45 PM.
This article is licensed under a Creative Commons Attribution 3.0 Unported Licence.

it into the body to treat specific cancer cells *via* external magnetic field guidance.[14] These spinach-derived nanoparticles are non-toxic and can be utilized for medicinal purposes in the pharmaceutical industry. Such a green synthesis of these nanoparticles represents an economically feasible production method.[15] An earlier study by Xu *et al.*[10] has already demonstrated the synthesis of carbon-based nanoparticles using spinach and polyethyleneimine, resulting in red fluorescence. However, those nanoparticles exhibited instability, gradually shifting from red to blue fluorescence within a week. To fabricate nanoparticles that exhibit red fluorescence over several months, we synthesized carbon nanoparticles *via* a simple and fast approach using microwave heating. Red fluorescent nanoparticles, especially under NIR excitation (800–1200 nm), are more advantageous than blue and green fluorescent nanoparticles because they can penetrate deep tissue with minimal auto-fluorescence and a high signal-to-noise ratio in biological tissues and fluids. Also, their requirement for a low excitation energy source does not damage cells or tissues, as seen in blue fluorescence. Blue fluorescence requires high-energy excitation, which can cause cell damage and cancer. Also, autofluorescence may occur as certain plant and animal tissues exhibit fluorescence when exposed to ultraviolet (UV) radiation, leading to interference with the signal of other CNPs.[16,17] Having said this, however, it remains difficult to synthesize red emissive CNPs with high quantum yield (QY) because the sp^2 π-conjugation domains are much larger, making them more prone to deformities and vulnerable to environmental disruption.[17–19]

We have synthesized novel red fluorescent carbon nanoparticles by a microwave synthesis route, as it combines the high reaction speed and uniform heating of the materials. The main benefit of employing microwave heating is the uniform, non-contact heat transfer to the solution, and its penetration characteristics enable the reactions to occur swiftly.[20] The microwave method is a highly effective procedure for nanoparticle synthesis, owing to its numerous benefits, such as being non-toxic, straightforward, scalable, and cost-effective. Nevertheless, the primary drawback of this technique is the limited ability to control the size of the resulting nanoparticles precisely.[21] The majority of synthesis methods involve temperatures of approximately 150 °C or higher, primarily hydrothermal and reflux methods. Furthermore, these methods typically require a minimum reaction time of 60 minutes or more, whereas implementing microwave-assisted approaches enables a significantly shorter reaction time of less than 30 minutes.

The carbon nanoparticles synthesized by this approach have a very high quantum yield of 94.67%, with high-intensity fluorescence in the near infrared region. Further characterization revealed that they are crystalline, showing good photostability. The emission is independent of the excitation wavelength, and the emission maxima are obtained at 672 nm when excited at a 410 nm wavelength. To utilize their nano-size, fluorescence properties, and biocompatibility, the uptake of the CNPs was studied as a bioimaging agent in a human cell line, Retinal Pigment Epithelium cells (RPE-1 cells), and in zebrafish larvae (Scheme 1). This study revealed that they are effective bioimaging agents showing bright red



Scheme 1 Red emissive carbon nanoparticles (CNPs) synthesized from the spinach (plant) source, demonstrating potential applications in bioimaging retinal pigment epithelium cells and zebrafish larvae. In addition, they have been shown to enhance wound closure in scratch assay experiments.

© 2023 The Author(s). Published by the Royal Society of Chemistry

Open Access Article. Published on 20 October 2023. Downloaded on 1/9/2025 7:18:45 PM.
This article is licensed under a Creative Commons Attribution 3.0 Unported Licence.

fluorescence inside the cells and larvae. As reported earlier,[22] the CNPs help in the wound-closure process, so a scratch assay was performed to investigate their effect on cell proliferation. The results showed that the wound closure rate in the control group was 40%, while it was 85% in the group treated with the CNPs. Increasing the concentration of CNPs also accelerated the wound-closure process. These findings indicate that the CNPs synthesized in this study have the potential as a theranostic agent and can be further modified for future biomedical applications.

2. Results and discussion

2.1 Synthesis and characterization of CNPs

Carbon nanoparticles emitting red fluorescence were synthesized through a microwave-assisted "green synthesis" approach from the ethanolic extract of spinach powder. 2 g of dried spinach leaf powder was mixed in 20 ml of ethanol solution and kept for stirring for 4 hours on a magnetic stirrer. The resulting mixture was centrifuged at 24 °C for 10 minutes at 10 000 rpm. A rota-evaporator was used to evaporate the ethanol from the supernatant. The resulting slurry was re-dispersed in 5 ml of Milli-Q water. The solution was subjected to microwave irradiation until the water evaporated. After cooling, 5 ml of ethanol was added and appropriately mixed, and the solution was set aside for 30 minutes. The solution was then probe-sonicated and then filtered using a 0.22 μm syringe filter. The solution was subsequently utilized to carry out further characterization and experimental research. To investigate the optical properties of the CNPs, we measured the absorption using UV-Vis (Ultraviolet-Visible) absorbance spectroscopy, which revealed distinctive peaks at 418 nm and 672 nm, corresponding to the level of energy transition associated with the angstrom-scale conjugated π-structure14 as depicted in Fig. 1(a). Several excitation wavelengths were used to determine the fluorescence emission spectra of red-emissive CNPs. Fig. 1(b) shows that the highest emission spectra (λ_{max}) were observed at 672 nm when excited at a 410 nm wavelength. The fluorescence upon excitation at 400 nm and 670 nm showed a single emission peak at 670 nm, as shown in the ESI,† Fig. S1 and S2. To learn more about the structure and composition of the CNPs, we carried out X-ray diffraction (XRD) and Fourier Transform Infrared (FT-IR) spectroscopy. X-ray diffraction (XRD) spectra show that they are amorphous. The XRD profile of the CNPs indicates that a broad peak at 22° is due to carbon (002 plane) suggesting their amorphous nature. In addition, the major peaks at 31.7° and small peaks at 27.4°, 45.4°, 53.7°, 56.4°, 66.2° and 57.3° are due to the presence of the NaCl salt[1] as shown in Fig. 1(c). The Fourier transform infrared (FTIR) spectra of the CNPs were recorded to detect the functional groups and chemical composition, as shown in Fig. 1(d). Chemical bonds between H, C, and O elements are usually formed in carbon-based nanoparticles. The following bands were observed in the spectra: C=C (1470 cm^{-1}), C–H bending (854 cm^{-1}), C–H stretching (2947, 2834 cm^{-1}), sp^2-CH and C–O stretching (1123, 1066, 1026 cm^{-1}). The absorption peak at 1470 cm^{-1} confirms the presence of C=C alkene; peaks at 1045.81 and 1085.16 cm^{-1} correspond to the C–O stretch ensuring that the carbonyl group is present; a peak at 854 cm^{-1} confirms the presence of C–H bending; and peaks at 2947 and 2834 cm^{-1} confirm that the alkyne group is present on the surface of the CNPs. The atomic force microscopy (AFM) image indicates a topological height of 3.14 nm, as shown in Fig. 1(e). As shown in Fig. 1(f), the particles' average size was 98 ± 20 nm when calculated using the ImageJ software. The CNPs with a production yield of 28 mg ml^{-1} and a quantum yield of 94.67% were obtained from an ethanolic extract of spinach powder (2 g). The photostability of the CNPs was measured for 50 minutes; the fluorescence decreased to 50% after 20 minutes as compared to that at time 0 minutes and after 50 minutes the fluorescence decreased to 90% as compared to that at time 0 minutes as shown in the ESI,† Fig. S3.

2.2 Optical properties of CNPs

We evaluated the UV-Vis absorption and fluorescence emission spectra to study the optical behavior. The prepared stock solution of concentration 28 mg ml^{-1} was further diluted in ethanol for further characterization. The fluorescence intensity is 1572 a.u. at 672 nm, as depicted in Fig. 1(b). The emission wavelength falls between 630 nm and 750 nm. The CNPs showed a green color under daylight and a bright red color under UV light. The CNPs exhibit an excitation wavelength-independent fluorescence spectrum profile. There was no apparent change in the emission profiles as the excitation wavelength increased. The QY is defined as the ratio of emitted photons to absorbed photons, which reflects the proportion of excited molecules that have returned to the ground state by releasing the emitted photons. Fluorescence emission experiments were carried out with a Jasco spectrofluorometer model FP-8300 (Japan) in the 410 nm excitation range. To record the emission spectra of CNPs, 10 mm path-length quartz cuvettes having a 10 nm slit width were used. According to the excitation spectra of CNPs, rhodamine B was chosen as the reference standard for calculating the QY of CNPs. The QY of the fluorescent CNPs is 94.67% in ethanol with respect to standard rhodamine B. The dispersion of the synthesized CNPs is more effective in protic solvents, such as alcohols, due to the formation of an H-bond with a nitrogen atom and the solvent molecule. As a result, it creates an inversion of the lowest-lying n–π* state to π–π*, resulting in a rise in fluorescence QY. The fluorescence quantum yield (QY) is a crucial factor for determining the performance of fluorescent probes used. QY is influenced by various environmental parameters such as temperature, viscosity, pH, H-bonding, solvent polarity, and quenchers, as well as fluorescence lifetime. Before utilizing CNPs as a fluorescent probe, it is essential to assess all these factors meticulously. CNPs' thermal stability was examined by exposing them to a temperature varying from 10 °C to 70 °C at intervals of 10 °C and by evaluating changes in their fluorescence spectra *via* a spectrophotometer. We can see from Fig. 2(a) that the increase in temperature caused a gradual reduction in fluorescence intensity, which can be attributed to

Open Access Article. Published on 20 October 2023. Downloaded on 1/9/2025 7:18:45 PM.
This article is licensed under a Creative Commons Attribution 3.0 Unported Licence.

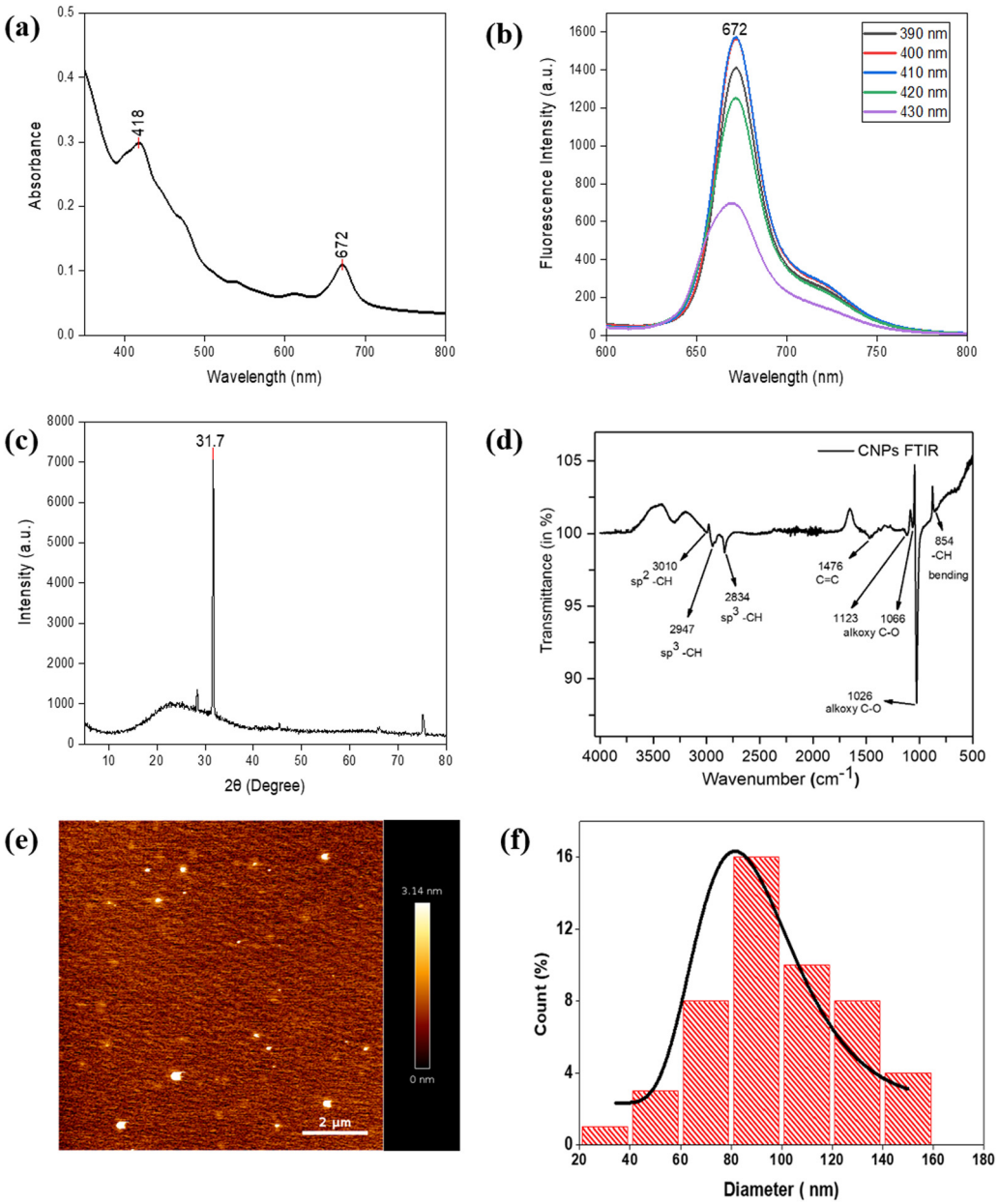


Fig. 1 Characterization of CNPs. (a) Ultraviolet (UV)-visible spectra of CNPs depicting two peaks at 418 nm and 672 nm related to different levels of electronic transitions. (b) The excitation and emission spectra of CNPs at the 410 nm excitation wavelength showed λ_{max} at 672 nm. (c) X-ray diffraction (XRD) analysis shows they are crystalline. The XRD profile of CNPs shows a broad peak at 22° due to carbon, major peaks at 31.7°, and small peaks at 27.4°, 45.4°, 53.7°, 56.4°, 66.2° and 57.3° due to the presence of the NaCl salt. (d) FTIR spectra reveal the chemical composition and functional groups of CNPs. (e) AFM of prepared CNPs using the microwave-assisted green synthesis route showed the particle size to be 98 ± 20 nm. (f) The statistical CNP size distribution was determined using the Image J software.

the presence of thermal energy inducing electronic vibrations that release non-radiative energy.[23] Furthermore, time-dependent fluorescence intensity was studied at 5 minute intervals over 30 minutes and it was found that the intensity remained constant over time, with the peak intensity consistent with that shown in Fig. 2(b). Our investigation on the effects of prolonged light exposure and temperature indicates that the CNPs synthesized exhibit good photostability and thermal stability with a slight decrement in intensity as the temperature rises.

2.3 Cellular uptake studies of CNPs

Confocal microscopy analyses were carried out on retinal pigment epithelial cells cultured with CNPs at varying concentrations to investigate their potential application in bioimaging. Experiments at different CNP concentrations of 50, 100, and 200 μg ml^{-1} for 30 minutes at 37 °C revealed that the CNPs were efficiently taken up by the cells and exhibited intracellular fluorescence. From inside the cells, the CNPs released a red fluorescence signal observed in the red channel and needed an excitation laser at 633 nm. As the amount of CNPs increased,

© 2023 The Author(s). Published by the Royal Society of Chemistry

Open Access Article. Published on 20 October 2023. Downloaded on 1/9/2025 7:18:45 PM.
This article is licensed under a Creative Commons Attribution 3.0 Unported Licence.

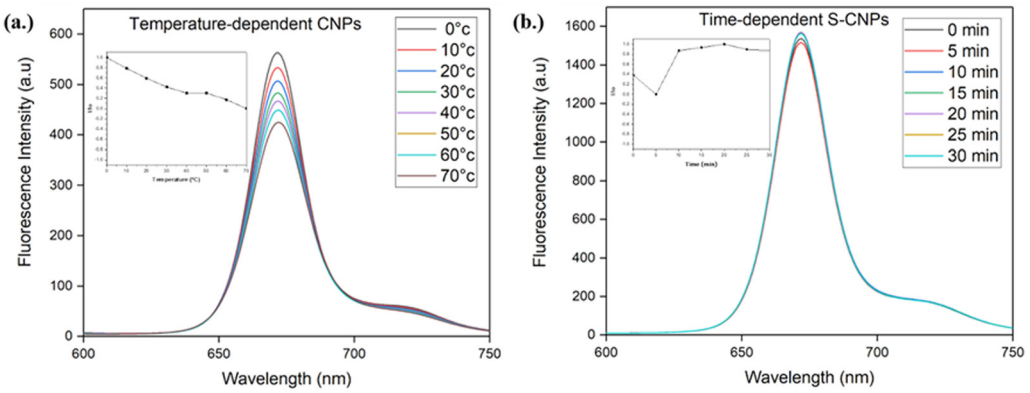


Fig. 2 (a) At varying temperatures (0–70 °C) the fluorescence spectrum of CNPs was measured with an increment of 10 °C. The fluorescence intensity marginally decreases from 10 °C to 70 °C as the temperature rises. (b) Fluorescence spectra at different durations (0–30 min) when maintained at 27 °C. Photostability of CNPs with respect to time is displayed in the inset.

the fluorescence signal was intensified, indicating a direct relationship between CNP concentration and intracellular fluorescence intensity. Using confocal data, we analyzed and quantified the results, indicating that cellular fluorescence intensity increased with increasing CNP concentration, showing a concentration-dependent absorption and fluorescence response. Through concentration-dependent studies, it has been revealed that as CNP concentrations increase from 50 to 200 g ml^{-1}, fluorescence intensity escalates, as depicted in Fig. 3.

2.4 Scratch test to study cell proliferation

Endocytosis is a process by which different ligands and nanoparticles are taken up by cells. These ligands and nanoparticles can trigger signalling events at the cell membrane, which can result in a variety of responses, including cell migration. To assess the uptake and role of CNPs in cell migration, we carried out a scratch assay test to investigate the wound-healing abilities of CNPs. To study the effect of cell migration on wound healing, we performed the assay in RPE-1 cells. This cell line has been explored previously for analyzing cell migration.[22] The RPE-1 cells were cultured in six-well plates, and when the cells attained full confluency, a wound-mimicking scratch was created using a 200 μL tip. It was found that the CNPs didn't hinder cell migration. To evaluate cell migration, the experiment comprised treating cells with CNPs at various concentrations and taking images at different time intervals.

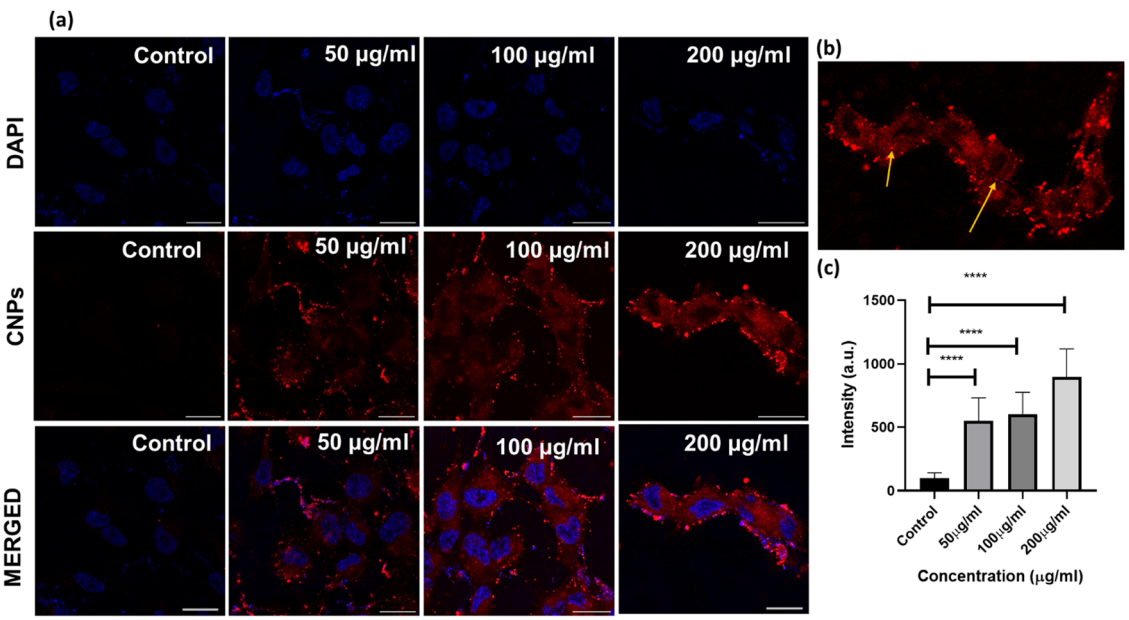


Fig. 3 (a) Confocal microscopy images show RPE-1 cells treated with CNPs at varying concentrations of 50, 100, and 200 μg ml^{-1}, with a corresponding control that was without CNPs, showing no fluorescence when excited at 633 nm. Studies on CNP concentration-dependent properties were conducted, and the results showed that the fluorescence intensity rises as the concentration of CNPs increases. (b) shows the puncta of CNPs inside the cells. The confocal image scale bar is held constant at 40 μm. (c) Using GraphPad prism software, CNP cellular uptake was also quantified at 50, 100, and 200 μg ml^{-1}. **** indicates a statistically significant value of $p < 0.0001$.

Open Access Article. Published on 20 October 2023. Downloaded on 1/9/2025 7:18:45 PM.
This article is licensed under a Creative Commons Attribution 3.0 Unported Licence.

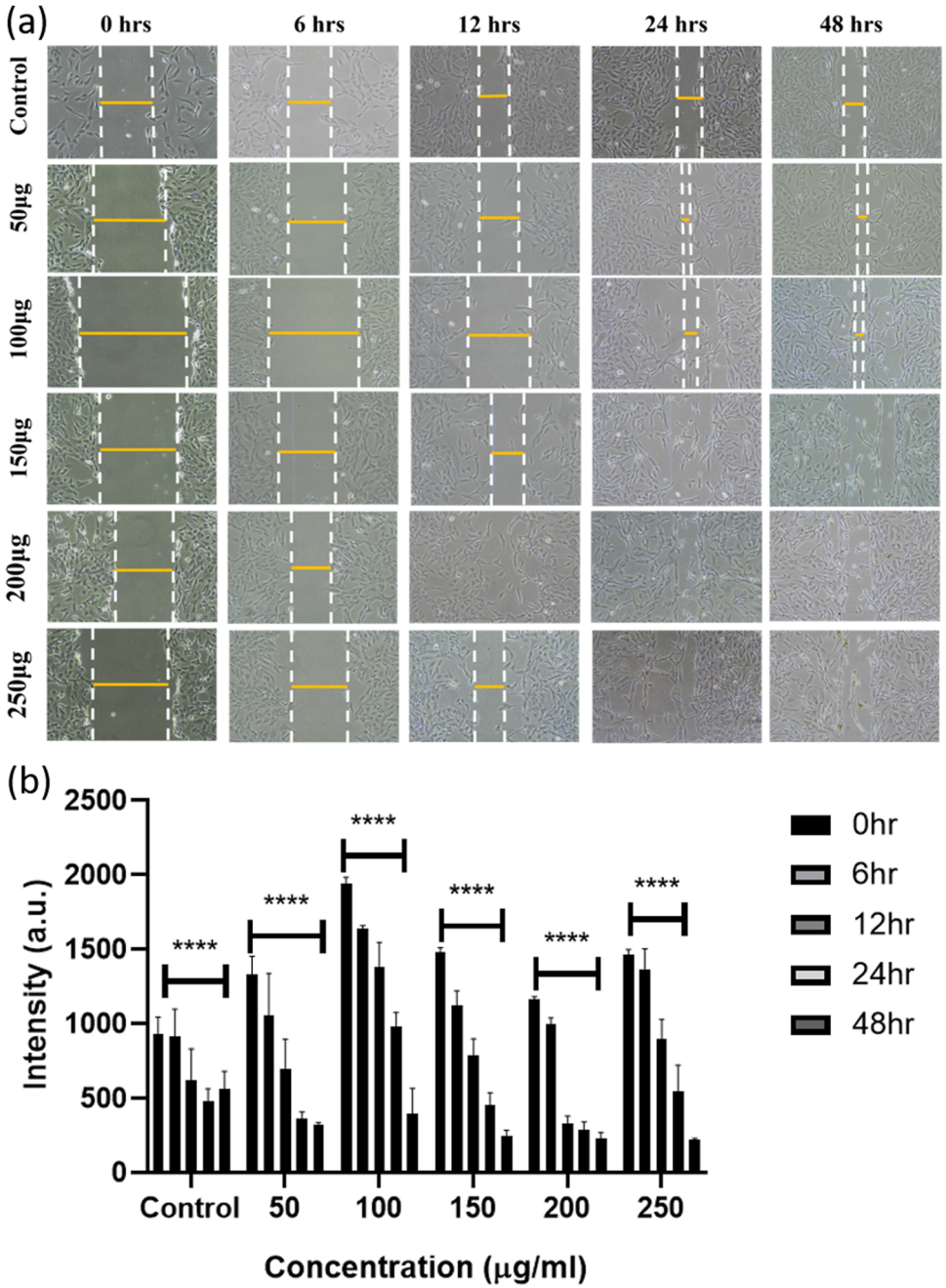


Fig. 4 (a) The wound-healing process of RPE-1 cells was imaged at different time points using a Nikon camera. The images were captured for control and cells treated with CNPs at concentrations of 50, 100, 150, 200, and 250 μg ml^{-1}. (b) Graph depicting that the wound healing process was accelerated with increasing concentrations of CNPs compared to the control group (without CNPs). Fiji ImageJ software was used for the quantification of the wound healing process in the presence of CNPs at 50, 100, 150, 200, and 250 μg ml^{-1} concentration. **** indicates a statistically significant value of $p < 0.0001$.

The findings revealed that there was an increase in cell migration and a faster wound healing response as the concentration of CNPs was increased from 50 μg ml^{-1} to 250 μg ml^{-1}, as shown in Fig. 4. In control, where no CNPs are added, the total wound healing is around 40%, whereas, in the presence of different CNPs, the wound closure process escalates with the increase in the concentration of CNPs with almost 85% of wound healing at 250 μg ml^{-1} concentration of CNPs.

2.5 CNP uptake in the zebrafish model system

To explore the *in vivo* imaging potential of developed CNPs, we studied the uptake in an animal model, where zebrafish larvae at 72 hours post-fertilization (hpf) were treated with varying CNP concentrations of 200 μg ml^{-1}, 300 μg ml^{-1} and 400 μg ml^{-1} for 4 hours. The finding indicates there was an increase in the uptake of CNPs as the concentration increased, which can be attributed to the improved bioavailability of these nanoformulations to the larvae. A statistically significant rise in

© 2023 The Author(s). Published by the Royal Society of Chemistry

Open Access Article. Published on 20 October 2023. Downloaded on 1/9/2025 7:18:45 PM.
This article is licensed under a Creative Commons Attribution 3.0 Unported Licence.

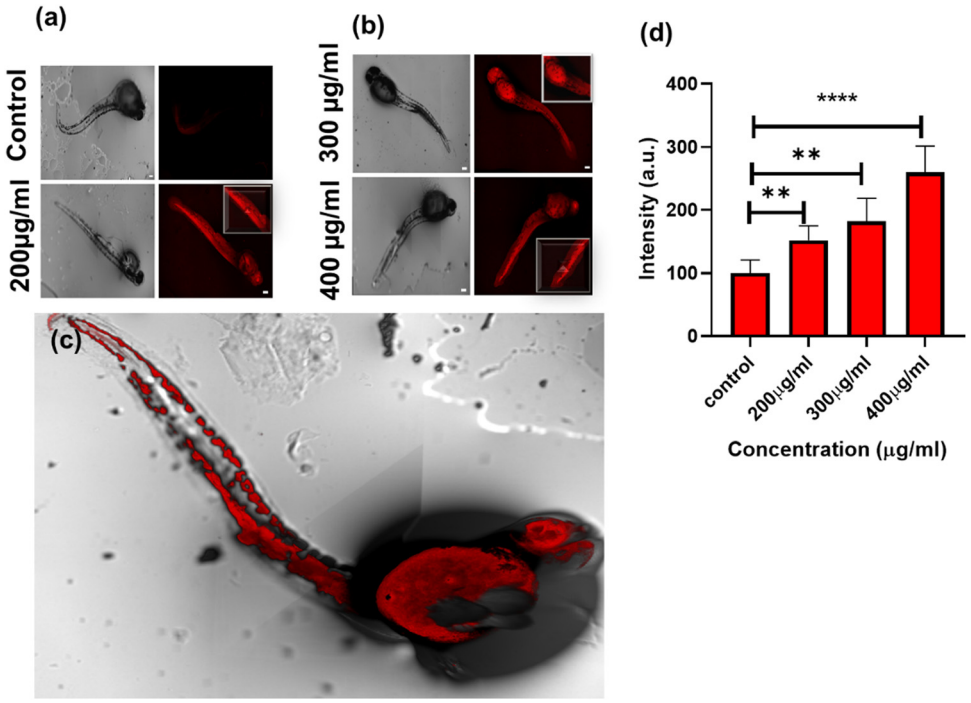


Fig. 5 Internalization studies of CNPs in zebrafish larvae. Different concentrations (200 μg ml^{-1}, 300 μg ml^{-1}, and 400 μg ml^{-1}) of CNPs were taken up by zebrafish larvae as shown in images (a) and (b). The zebrafish larvae were treated for 4 h with each concentration. (c) shows the 3D image of the uptake of CNPs by zebrafish larvae. A quantification study of the internalization of CNPs is shown in graph (d). The scale bar is set at 100 μM. ** denotes a statistically significant p-value ($p < 0.01$). **** denotes a statistically significant p-value ($p < 0.0001$). 06 larvae were analyzed per condition.

the fluorescence intensity of the CNPs was seen at four hours post-treatment compared to the control. Furthermore, the CNPs were found to be uniformly distributed throughout the zebrafish, including the yolk sac, head, and tail regions, indicating their efficient uptake, as we can see in Fig. 5. These findings suggest that the CNPs possess bioaccumulation properties and validate their potential for bioimaging.

3. Conclusions and discussion

The current study presents a facile and environmentally friendly method for synthesizing carbon nanoparticles using *Spinacia oleracea* leaf extracts. The resulting red-emissive carbon-based nanoparticles exhibit bright red luminescence in the near-infrared (NIR) region, with an emission maximum of 672 nm and a high quantum yield of 94.67%. The synthesized CNPs have demonstrated remarkable properties, have a nano-size range, and have exhibited excellent photostability over long-term storage. Overall, CNPs are amorphous, having NaCl impurity. The surface of CNPs has various chemical functional groups, for example, C–O, C═C, and C–H. The emission spectra of the CNPs, upon excitation from 390 nm to 430 nm, show a peak at 670 nm, with maximum emission upon excitation at 400 nm. The shape of the CNPs is disc-type, having a size of 98 nm and a height of 3.14 nm. The studies on CNPs also reveal their significant uptake by both RPE1 cells and zebrafish larvae, highlighting their potential as a targeted bioimaging agent in diverse biomedical applications. Scratch assay analysis demonstrates that higher concentrations of CNPs (ranging from 50 μL to 250 μL) led to increased cell migration and faster wound-closure response within 48 hours. Thus, it can be concluded that the CNPs promoted cell migration more effectively than the control group, indicating that they are biocompatible, and can accelerate wound healing, and thus can be potentially used as a bioimaging agent for various biological applications, including tissue engineering and regenerative medicine. Future studies will focus on maximizing their uptake efficiency and investigating their compatibility with diverse *in vivo* biological systems. Additionally, generating nanoparticles for theranostic applications combining diagnostic and therapeutic roles could be a fruitful avenue for research. For example, conjugating drugs with nanoparticles could enable targeted drug delivery and monitoring of treatment efficacy in real-time. Thus, there is a potential future for the biosynthesized carbon nanoparticles in biomedical applications, which can serve as a benchmark for researchers to promote sustainability in the field of nanotechnology.

4. Materials and methods

4.1 Materials

Fresh spinach leaves were obtained from a vegetable vendor located at IIT Gandhinagar, Gujarat, India. The experiment utilized deionized water obtained from Merck Millipore; absolute ethanol (>99.9%) was supplied by Changshu Hongsheng Fine Chemicals Co., Ltd; rhodamine B was purchased from

Open Access Article. Published on 20 October 2023. Downloaded on 1/9/2025 7:18:45 PM. This article is licensed under a Creative Commons Attribution 3.0 Unported Licence.

HiMedia; and syringe filters were procured from Merck. Dulbecco's modified Eagle's medium (DMEM), penicillin–streptomycin, trypsin–EDTA (0.25%), and fetal bovine serum (FBS) were obtained from Gibco and were of excellent scientific grade, requiring no additional sterilization or treatment.

4.2 Synthesis of fluorescent CNPs

A microwave approach was used to synthesize red fluorescence-emitting carbon nanoparticles. In a clean, dirt-free glass vial, 2 g of spinach powder was mixed in 20 ml of ethanol solution and kept for 4 hours for stirring on a magnetic stirrer. The resulting mixture was centrifuged at 24 °C for 10 minutes at 10 000 rpm. A rota-evaporator was used to evaporate the ethanol from the supernatant. The resulting slurry was re-dispersed in 5 ml of Milli-Q water. The solution was subjected to microwave irradiation until the water evaporated. After cooling, 5 ml of ethanol was added and appropriately mixed, and the solution was set aside for 30 minutes. The solution was then probe-sonicated and then filtered using a 0.22 m syringe filter. The synthesized nanoparticles dissolved in ethanol were used for further experiments.

4.3 Analytical methods used to study the characterization of CNPs

Two-dimensional and three-dimensional images of CNPs were obtained using an atomic force microscope (Bruker Multimode 8). To analyze the crystalline properties of the CNPs, a Bruker-D8 DISCOVER X-ray spectrometer and Cu-Kα radiation were used to perform X-ray diffraction experiments. The diffraction scans were taken over a range of 5° to 80° with a scanning rate of 0.2° min^{-1}. Using a Jasco FP-8300 spectrofluorometer (Japan), the CNPs were excited in the 400–500 nm region. Rhodamine B was taken as the standard reference for calculating the relative QY, and it was discovered that the CNPs had a quantum yield of 94.67% in ethanol. Using a Spectro Cord-210 Plus Analytik Jena UV-Vis spectrophotometer made in Germany, the CNP's UV-Vis absorbance spectra were recorded. The FTIR of CNPs was conducted in ATR (attenuated total reflectance) mode using a Spectrum 2 FTIR spectrometer from PerkinElmer. The scanning range for the measurements was 1000 cm^{-1} to 4000 cm^{-1}.

4.4 Spectroscopic studies

The absorbance and emission spectra were recorded in spectroscopic-grade solvents. The emission spectra were recorded at 10 nm following the excitation wavelength for recording the standard emission spectra. The relative quantum yield of CNPs was calculated using rhodamine B as a reference.

The following equation is used to calculate quantum yield:

$$QY = QY_R \times \frac{I \times OD_R \times n^2}{I_R \times OD_R \times n_R{}^2}$$

where quantum yield is denoted as QY, integrated fluorescence intensity is shown as I, OD stands for optical density, n is the refractive index, and R indicates the reference.

4.5 Cell culture

Professor Ludger Johannes graciously provided retinal pigment epithelial cells, RPE1, from Institut Curie in Paris, France. This cell line was cultured in complete DMEM media, and 1× PBS with a pH of 7.4 was used in all experiments.

4.5.1 Confocal microscopy studies. RPE1 cells were seeded at a density of approximately 40 000 cells per well onto coverslips in 24-well cell culture plates containing DMEM cell culture media. The cells were then incubated for 24 hours at 37 °C with 5% CO_2. Once full confluency of the RPE1 cells had reached, they were treated with PBS and then subjected to three different doses of CNPs (50, 100, and 200 μg ml^{-1}) for 30 minutes. The cells were subsequently fixed with 4% PFA for around 20 minutes after being rinsed twice with PBS. After fixing, the cells were washed thrice with PBS to remove any remaining particles and PFA. DAPI stain was used to stain the fixed cells, and a mounting medium (Mowoil) was used to mount them on glass slides. An oil immersion objective 63× Leica TCS SP5 confocal microscope was used to examine the cellular internalization of CNPs. A 405 nm laser was used as the excitation source for DAPI, whereas a 633 nm laser was employed for the excitation of nanoparticles. For DAPI and carbon nanoparticles, the emission bandwidths were tuned accordingly at 410–450 nm and 644–800 nm.

4.5.2 Zebrafish husbandry and maintenance. Zebrafish of Assam wild type were bought from local vendors. They were retained in under-regulated laboratory settings at Ahmedabad University by the procedure described by Kansara *et al.*, 2019.[24] In artificially created freshwater, male and female fish were kept in 20 L tanks with the quality of water maintained as per ZFIN standards. Using a multi-parameter device PCD 650 Model, Eutech, India, water parameters such as TDS (220–320 μg ml^{-1}), pH (6.8–7.4), dissolved oxygen (>6 μg ml^{-1}), conductivity (250–350 μg ml^{-1}), and salinity (210–310 μg ml^{-1}) were frequently examined. Zebrafish embryos were acquired and cultured for the experiment in the E3 medium, composed of deionized water containing 0.33 mmol L^{-1} $CaCl_2$, 0.17 mmol L^{-1} KCl, 0.33 mmol L^{-1} $MgSO_4$ and 5 mmol L^{-1} NaCl, and the pH of the E3 medium was adjusted to 7.2 before autoclaving the E3 medium. The embryos were maintained at 28 °C during the experiment. The pH of the E3 medium was adjusted to 7.2, and it was autoclaved and stored at room temperature. The incubation was carried out at 28 °C.

4.5.2.1 In vivo studies on zebrafish larvae. The uptake analyses were conducted utilizing zebrafish larvae at 72 hours post-fertilization (hpf) based on the recommendations of the Organization for Economic Cooperation and Development (OECD). Live larvae were added to six-well plates containing 15 larvae per well after dead larvae were removed. The bioimaging potential of the CNPs was evaluated in larvae by administering varying concentrations (200, 300, and 400 μg ml^{-1}) of the nanoparticles in each batch. One set of control wells was kept, where larvae were not exposed to the CNPs. The other set comprises varying concentrations of CNPs. After the CNP treatment, excess CNPs were removed by washing the larvae

© 2023 The Author(s). Published by the Royal Society of Chemistry

twice with the E3 medium. The larvae were then placed on a glass slide *via* mounting Mowiol solution after being fixed with 4% PFA solution for approximately two to three minutes. The slides were then analyzed for confocal imaging after being air-dried.

Conflicts of interest

The authors declare no conflict of interest.

Acknowledgements

We sincerely thank all the members of the DB group for critically reading the manuscript and for their valuable feedback. KB thanks D. Y. Patil Vidhyapeeth, Pune. US thanks IITGN-MHRD, GoI for PhD KK thanks SERB, GoI for the National Postdoctoral Fellowship. DB thanks SERB, GoI for the Ramanujan Fellowship, IITGN for the startup grant, and DBT-EMR, Gujcost-DST and GSBTM for research grants. Imaging facilities of CIF at IIT Gandhinagar are acknowledged.

References

1 R. Atchudan, T. N. J. I. Edison, S. Perumal, R. Vinodh and Y. R. Lee, Betel-derived nitrogen-doped multicolor carbon dots for environmental and biological applications, *J. Mol. Liq.*, 2019, **296**, 111817.
2 R. Atchudan, T. N. J. I. Edison, S. Perumal, N. Muthuchamy and Y. R. Lee, Hydrophilic nitrogen-doped carbon dots from biowaste using dwarf banana peel for environmental and biological applications, *Fuel*, 2020, **275**, 117821.
3 P. Krishnaiah, *et al.*, Utilization of waste biomass of Poa pratensis for green synthesis of n-doped carbon dots and its application in detection of Mn^{2+} and Fe^{3+}, *Chemosphere*, 2022, **286**, 131764.
4 N. Baig, I. Kammakakam and W. Falath, Nanomaterials: a review of synthesis methods, properties, recent progress, and challenges, *Mater. Adv.*, 2021, **2**, 1821–1871.
5 M. Asnawi, S. Azhari, M. N. Hamidon, I. Ismail and I. Helina, Synthesis of Carbon Nanomaterials from Rice Husk via Microwave Oven, *J. Nanomater.*, 2018, **2018**, 1–5.
6 R. Atchudan, *et al.*, Highly fluorescent nitrogen-doped carbon dots derived from Phyllanthus acidus utilized as a fluorescent probe for label-free selective detection of Fe^{3+} ions, live cell imaging and fluorescent ink, *Biosens. Bioelectron.*, 2018, **99**, 303–311.
7 R. Atchudan, *et al.*, Tunable fluorescent carbon dots from biowaste as fluorescence ink and imaging human normal and cancer cells, *Environ. Res.*, 2022, **204**, 112365.
8 P. Yadav, *et al.*, Tissue-Derived Primary Cell Type Dictates the Endocytic Uptake Route of Carbon Quantum Dots and *In Vivo* Uptake, *ACS Appl. Bio Mater.*, 2023, **6**, 1629–1638.
9 M. Han, *et al.*, Recent progress on the photocatalysis of carbon dots: Classification, mechanism and applications, *Nano Today*, 2018, **19**, 201–218.
10 X. Xu, *et al.*, Red-emissive carbon dots from spinach: Characterization and application in visual detection of time, *J. Lumin.*, 2020, **227**, 117534.
11 R. Mohammadinejad, S. Karimi, S. Iravani and R. S. Varma, Plant-derived nanostructures: types and applications, *Green Chem.*, 2016, **18**(1), 20–52.
12 M. L. Liu, B. B. Chen, C. M. Li and C. Z. Huang, Carbon dots: synthesis, formation mechanism, fluorescence origin and sensing applications, *Green Chem.*, 2019, **21**(3), 449–471.
13 G. E. Hoag, J. B. Collins, J. L. Holcomb, J. R. Hoag, M. N. Nadagouda and R. S. Varma, Degradation of bromothymol blue by 'greener'nano-scale zero-valent iron synthesized using tea polyphenols, *J. Mater. Chem.*, 2009, **19**(45), 8671–8677.
14 B. Fayyaz, M. B. Zahra and M. S. Haider, *Screening of Phenolic Compounds from Spinach (Spinacia oleracea), Green Synthesis of Iron-Nanoparticles and Determination of its Anti-Microbial Effect on Escherichia coli*, 2022.
15 M. Mahdavi, M. B. Ahmad, M. J. Haron, F. Namvar, B. Nadi, M. Z. A. Rahman and J. Amin, Synthesis, surface modification and characterisation of biocompatible magnetic iron oxide nanoparticles for biomedical applications, *Molecules*, 2013, **18**(7), 7533–7548.
16 K. Barve, U. Singh, P. Yadav and D. Bhatia, Carbon-based designer and programmable fluorescent quantum dots for targeted biological and biomedical applications, *Mater. Chem. Front.*, 2023, **7**(9), 1781–1802.
17 W. Liu, *et al.*, Carbon dots: surface engineering and applications, *J. Mater. Chem. B*, 2016, **4**(35), 5772–5788.
18 Z. Wang, F. Yuan, X. Li, Y. Li, H. Zhong, L. Fan and S. Yang, 53% efficient red emissive carbon quantum dots for high color rendering and stable warm white-light-emitting diodes, *Adv. Mater.*, 2017, **29**(37), 1702910.
19 S. K. Bhunia, A. Saha, A. R. Maity, S. C. Ray and N. R. Jana, Carbon nanoparticle-based fluorescent bioimaging probes, *Sci. Rep.*, 2013, **3**(1), 1473.
20 S. Mehta, K. Barve, U. Singh and D. D. Bhatia, Psidium guajava derived carbon nanoparticles: A promising red emissive cellular bioimaging agent, *bioRxiv*, 2023, preprint, DOI: **10.1101/2023.03.20.533411**.
21 M. Farshbaf, S. Davaran, F. Rahimi, N. Annabi, R. Salehi and A. Akbarzadeh, Carbon quantum dots: recent progresses on synthesis, surface modification and applications, *Artif. Cells, Nanomed., Biotechnol.*, 2018, **46**(7), 1331–1348.
22 U. Singh, K. Shah, K. Kansara, A. Kumar and D. D. Bhatia, A novel class of greenish-yellow emitting carbon dots stimulates collective cell migration and 3D uptake in vivo, *ChemNanoMat*, 2023, e202200572.
23 I. Marica, F. Nekvapil, M. Ştefan, C. Farcău and A. Falamaş, Zinc oxide nanostructures for fluorescence and Raman signal enhancement: a review, *Beilstein J. Nanotechnol.*, 2022, **13**(1), 472–490.
24 K. Kansara, *et al.*, A critical review on the role of abiotic factors on the transformation, environmental identity and toxicity of engineered nanomaterials in aquatic environment, *Environ. Pollut.*, 2022, **296**, 118726.

Open Access Article. Published on 20 October 2023. Downloaded on 1/9/2025 7:18:45 PM. This article is licensed under a Creative Commons Attribution 3.0 Unported Licence.